Additive Manufacturing of Carbon Steels Through Direct Ink Write Printing of Oxide Precursors.

A Thesis

Presented to

The Academic Faculty

by:

Collin Stiers

In Partial Fulfillment

of the Requirements for the Degree

Master of Science

in the

School of Materials Science and Engineering

Georgia Institute of Technology

May 2022

Additive Manufacturing of Carbon Steels Through Direct Ink Write Printing of Oxide Precursors.

Approved by:

Dr. Joshua Kacher, Advisor
School of Material Science and Engineering
Georgia Institute of Technology

Dr. Naresh Thadhani
School of Material Science and Engineering
Georgia Institute of Technology

Dr. Blair Brettmann
School of Chemical and Biological Engineering and
School of Material Science and Engineering
Georgia Institute of Technology

Date Approved: 05,13,2022

Acknowledgments

The completion of this thesis would not have been possible without the incredible support of many people. First, I would like to thank my adviser Dr. Josh Kacher for his advice and guidance throughout this process, without his help I would never have been able to grow into not just an engineer but also a material scientist. Second, I would like to thank my committee members Dr. Naresh Thadhani and Dr. Blair Brettman for their feedback and advice. Dr. Brettman specifically was also an invaluable consultant on this work whose knowledge of polymers and solvents was incredibly helpful.

A special thanks is owed to Katie Koube, without whom I would never have even started work in the Kacher Lab, much less aspired to attend graduate school. Katie has displayed superhuman patience as I floundered my way through a transition from mechanical engineering to material science. She has taught me more than perhaps any other individual at Georgia Tech, both personally and professionally and I have the honor of also considering her a great personal friend.

I also owe much gratitude to wonderful colleagues who have been invaluable to my research and professional development, including Ethan Sinclair, Hyoungjun Sim, Aashray Narla, Dr. Jahnavi Desai, Bruno Geoly, and Josie DeRonja.

Finally, I would like to gratefully acknowledge the funding provided for this research by the Georgia Tech Research Institute HIVES grant, and the United States Special Operations Command Ignite program.

Contents

List of Tables

List of Figures

Summary

A method for additive manufacturing of various carbon steels from low cost and stable oxide powders is presented. This method uses direct ink write (DIW) processes to extrude inks composed of oxide powders, plastic binders, and solvents. Oxide powders are synthesized into viscous inks through mechanical mixing with a plastic binder and solvents. Inks are then extruded under ambient conditions into three dimensional (3D) architectures. The 3D printed green bodies solidify on contact with air after which they are subjected to a reducing process at elevated temperatures in hydrogen-rich environments to burn off the polymer binder and reduce the oxide powders, yielding metal alloys with controlled compositions. While this approach has been demonstrated in previous publications for various alloys, adding carbon, an important element in most industrial steels, has been a persistent challenge. This paper demonstrates an approach to introduce carbon during the reduction process, resulting in through-thickness carburization of the final parts. Post-printing, the parts can be heat treated to achieve desirable characteristics through well-established methods

Chapter 1: Introduction and Research Objectives

Carbon steel is one of the most ubiquitous engineering materials in the modern world, and accounts for a large portion of all alloys used today.[1] The manufacture of carbon steel is a well-developed technology and has remained fundamentally unchanged for decades. Metal ores such as hematite, magnetite, and limonite are melted together.[2] they are then combined with coke and limestone, and excess oxides and carbon are removed from the melt mixture, either as slag or off-gassing, yielding a metallic alloy with the appropriate amount of carbon.[3] The addition of carbon to iron alloys has tremendous beneficial effects, including increased ultimate tensile strength, yield strength, and modulus.[4],[5],[6] Carbon also increases the hardness of the alloy, and hardness is related to a range of desirable properties including surface wear resistance.[7] The unfortunate downside to increased carbon content in a decrease in the weldability of the steel.[8],[9] This decreased weldability also has repercussions for the additive manufacturing of steels.[10]

Additive manufacturing (AM) is seeing increased industrial application due to its ability to rapidly fabricate parts with complex geometries. The most common method of metal AM is Laser Powder Bed Fusion (L-PBF),[11] which relies on high powered lasers to sinter powder layers in defined patterns, building the desired geometry layer by layer. This fabrication approach introduces rapid heating/cooling cycles, similar to those found in welding, which leads to thermal stresses and cracking in many industrial alloys, including the carbon steels alloys presented in this paper.[12] Current industrial applications of L-PBF are limited by the high costs to produce parts, with the price influenced heavily by the cost of powdered metal alloys. L-PBF also has geometric limitations. Parts are sintered on a powder bed layer by layer, with new powder being deposited

after each step.[13] This requires that parts be designed with a way to remove unsinttered powders, and doesn't allow for the creation of closed, or hollow parts, or tight porous structures of the kind often used as infill for polymer 3D printing.[14,15]

The research objective of this work includes the production of high carbon steels, from cheap and readily available oxide precursors, and evaluation of the carbon content and density of printed parts.

Chapter 2: Background

There is clear utility in developing effective methods to 3D print carbon steels. However, additive manufacturing of carbon steels has proven a consistent challenge. The conventional industrial mechanisms of steel production in a blast furnace cannot be applied directly to additive manufacturing. AM methods cannot produce the environmental condition of a steel blast furnace.[16],[17] They are therefore unable to produce the temperatures necessary to melt or sinter the iron oxides present in iron ores.[18],[19] Variations of L-PBF are the most widely used methods of metal additive manufacturing,[11] but printing of carbon steels using these methods has been largely limited to low carbon steels (less than .2 wt% C).[20] The higher carbon content present in medium and high carbon steels decreases weldability and interferes with sintering required for L-PBF and other energy based printing approaches.[21,22] Higher carbon steels printed in this manner have greater amounts of porosity and increased cracking. Additionally, the preparation of powders suitable for L-PBF is expensive and inflexible. A single steel alloy must be produced through conventional means, gas atomized, sieved for size, and contained in an inert environment to prevent oxidation and potential conflagration before being printed.[23] This process limits flexibility and customizability of alloy compositions, as fabricating powders for new alloys is expensive and

time consuming. Wire arc additive manufacturing solves these powder issues, but weldability issues remain and so this technique is still limited to very low carbon steels.[24]

Filaments for fused deposition modeling methods have been developed to print medium carbon steels from pre-alloyed metal powders. However post processing times for these methods range from 29 to 103 hours, making widespread use and scalability of this method difficult [25,26] Further, similar to L-PBF, these AM methods use metal powders, which are difficult and dangerous to store and transport in large quantities, expensive to manufacture, and easily damaged by exposure to air.

2.1: Oxide Direct Ink Write (DIW)

AM and the subsequent reduction of oxides through oxide DIW is an established and effective method of creating complex architectures of various metals and alloys.[27] In this approach low-cost, stable oxide powders are mechanically mixed with graded volatility solvents and a plastic binder to create a viscous, printable, shear thinning, ink.[28] The ink is then printed in ambient conditions to create a robust oxide green body. The highest volatility solvents flash off on contact with air and cause the inks to harden, while other solvents remain for a longer time to allow for bonding of adjacent, and following, printed lines and layers.[28] The part fully hardens during the print to form a stable green body, which is then post processed at elevated temperature in a reducing environment. The plastic binder is burned off and the oxides are reduced in hydrogen to create a pure metal or alloy, with the composition dictated by the ratio of oxide powders used in the build. Samples at different stages in this process can be seen in **Figure 1.** It should be noted that the process of preparing the inks for printing is not linked to the specific oxide mix. The amount of all the components for the ink are based on the volume of oxide powder. Within that volume the alloy composition can simply be changed by adding different oxide powders, as the

oxide powders are first mixed in by hand, batches of a variety of alloys can be produced in almost any size.

While this approach has been demonstrated for a wide range of metals and alloys,[27] introducing carbon into the available compositions has been a persistent challenge. Oxide DIW is a promising candidate for the production of carbon steels as parts are reduced and sintered in a furnace, which avoids the weldability issues associated with the rapid heat/cool cycles in other methods of additive manufacturing.

Figure 1: A: Sample after printing. **B:** Samples after furnace processing. **C:** Samples mounted and ground for hardness testing

2.2: Reduction and Oxide selection

The specific composition of metals and alloys printed using oxide DIW is based on the suitability of different metal oxides to be reduced in hydrogen. The Ellingham diagram in **Figure 2** shows the favorability of reduction reactions for various oxides across different temperatures. Only metal oxides that are relatively reduceable in H_2 can be used. These are those oxides that are above the "hydrogen line" (highlighted in green) on the Ellingham diagram, namely iron (III) oxide (Fe_2O_3), and nickel (II) oxide (NiO) were selected for the alloys used in this thesis. However cobalt and copper oxides are both above the hydrogen line as well. Prior research in the field of metal reduction in H_2 indicates that a wide range of important steel alloys can be produced by reduction of their constituent oxides.[29] Oxides that fall below the H_2 line on the

Ellingham diagram have more negative Gibbs free energy. Some, such as Al_2O_3 are far too stable to be reduced in H_2 and will melt before reduction occurs. Other oxides relevant to production of various steels such as Cr, Mn, and Mo fall below this line, and therefore one might expect that they cannot be reduced, however prior work has shown that by altering the local thermodynamic environment,

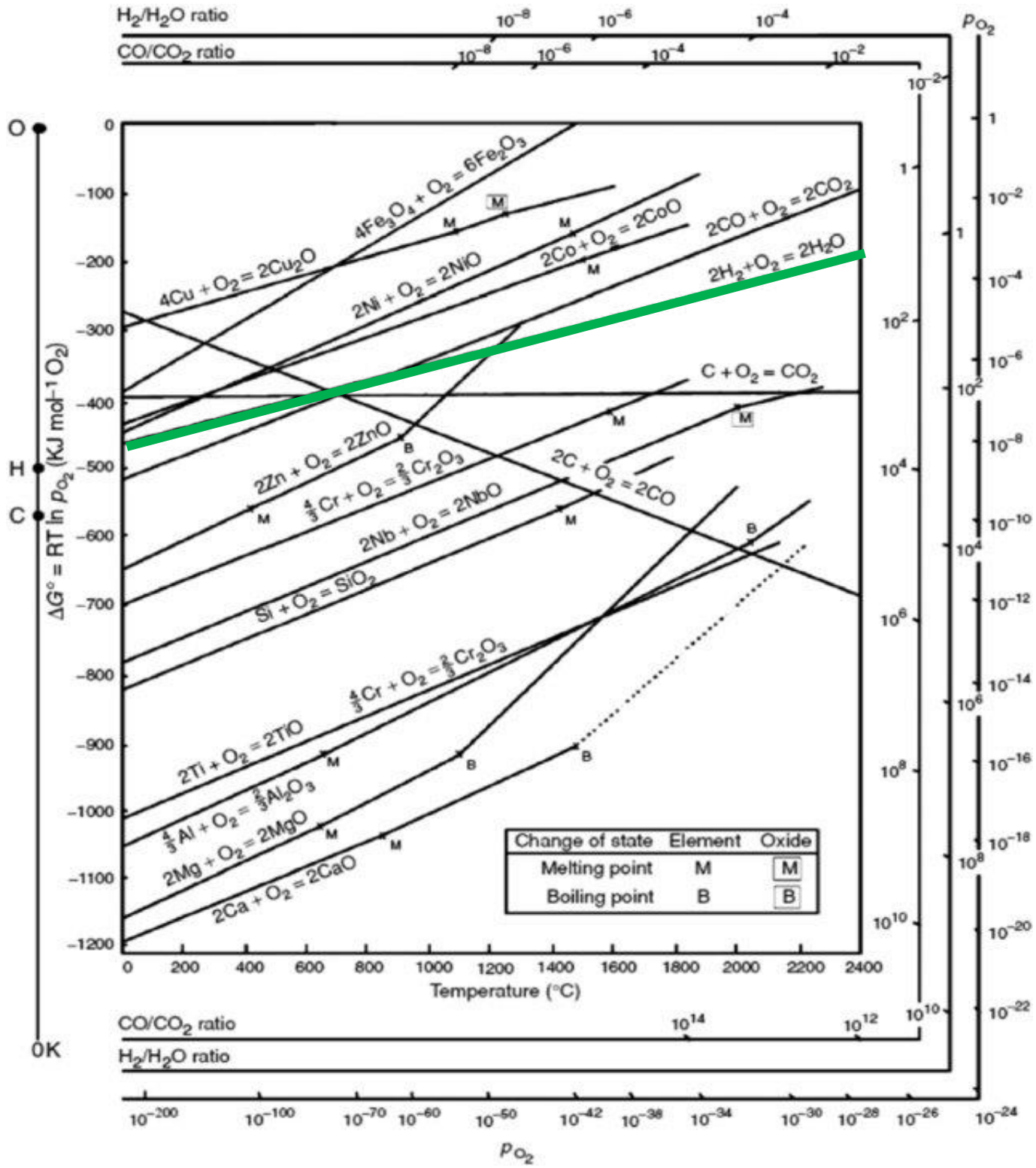

Figure 2: Ellingham Diagram[30,31]

specifically with the presence of nickel, these oxides can be reduced.[32,29,33] This indicates that there is a possibility for wide ranging applications of the methods presented to here, to a variety of steel alloys not explored in this work. Consideration of the reducibility of oxides will be important in future work on the production of various steel alloys through oxide DIW.

The furnace post processing procedure used to reduce and sinter oxide green bodies depends on the specific composition of the oxide mix. Some prior work has been used as a starting point for the processes used in this work and is shown in **Figure 3.**

2.3: Carburization of steels

Carburization of steels is an incredibly old technology dating back to the ancient Greeks.[37] In carburization, a steel part with low carbon content is in some way exposed to a carbon rich environment, and this carbon is allowed to diffuse inward from the surface of the part, forming a carbon rich outer layer.[38] Carburization is generally viewed as a case hardening process, as the diffusion process is quite slow and only the surface of the part generally has enough carbon in it to be hardened.[39]

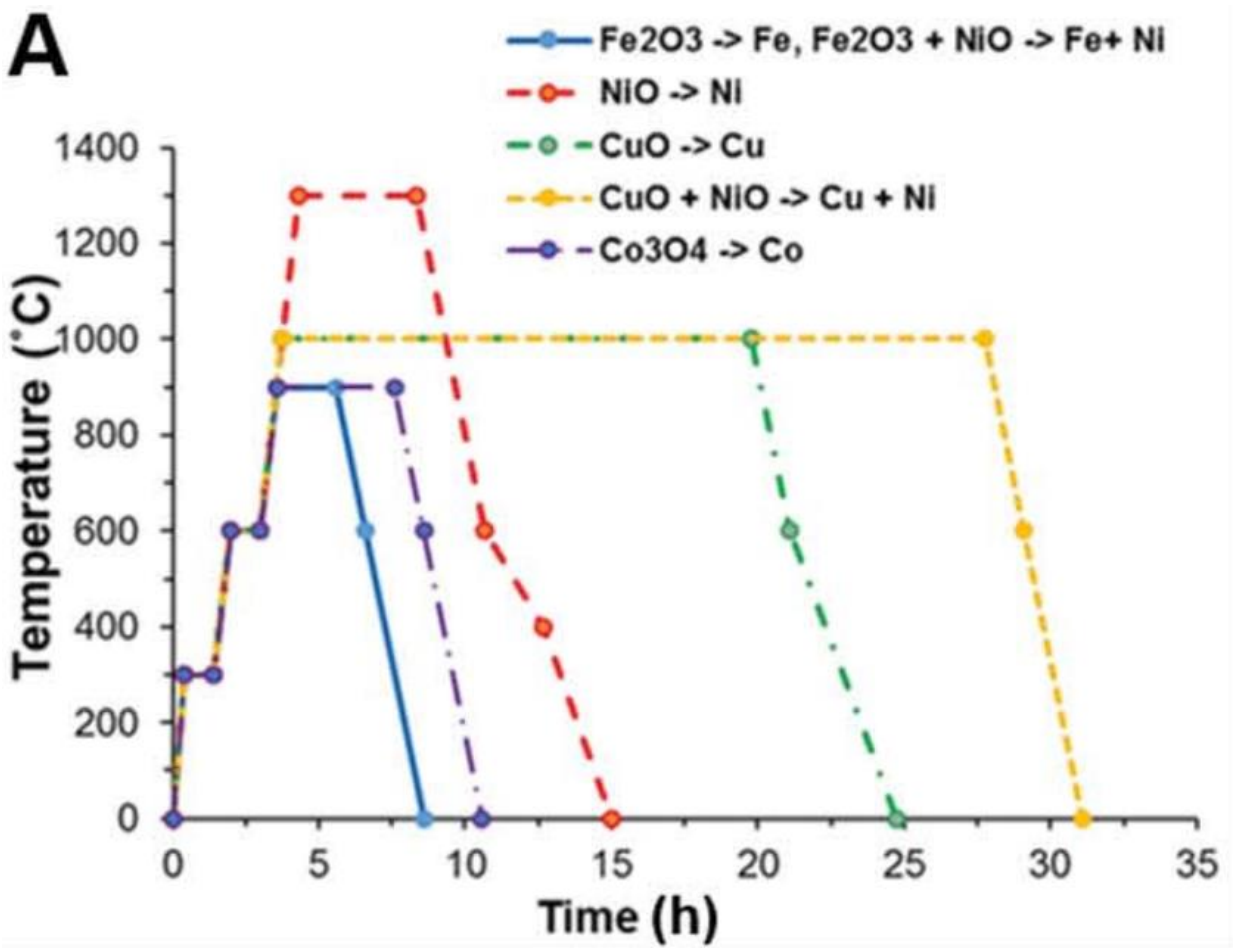

Figure 3: Furnace post processing procedure for various alloys[27]

2.3.1: Pack Carburization

Pack carburization is a carburizing process in which the carbon rich environment is provided by a solid compound packed around the part to be hardened. It is possible to achieve carburization by surrounding a part in pure powdered carbon.[40] However, this is relatively slow and inefficient because for pack carburizing to effectively carburize the samples, solid carbon must first be converted into CO.[41] Solid carbon is not mobile enough to diffuse directly into the metal. Typically, pack carburizing occurs in an environment where the solid carbon can be directly exposed to atmospheric O_2, this reacts to form CO, which then can react with the metallic iron to

deposit active carbon onto the metallic surface which will then diffuse inside, as seen in equations 1-3.[42]

$$2C + O_2 \rightarrow 2CO \quad \text{(Eq 1)}$$

$$2CO + Fe \rightarrow C_{active} + CO_2 \quad \text{(Eq 2)}$$

$$CO_2 + C \rightarrow 2CO \quad \text{(Eq 3)}$$

Commercial pack carburizing compounds also contain 'energizers', which are forms of carbonate that exist to bias the above reactions to the production of CO rather than CO_2 or H_2O. These carbonates do not fully break down in any one pack carburizing process and can be reused many times. Generally pack carburizing compounds are formed primarily out of coke or hardwood charcoal, with the addition of approximately 15% by weight of carbonates, usually in the form of barium carbonate.[43] However, barium carbonate is toxic and is generally being phased out in favor of other carbonates such as calcium carbonate.

The rate of carburization depends on many factors including the composition of the carburizing compound and the temperature at which carburization occurs. A representative example of the depth of carbon penetration from pack carburizing for various carburization times can be seen in **Figure 4.**

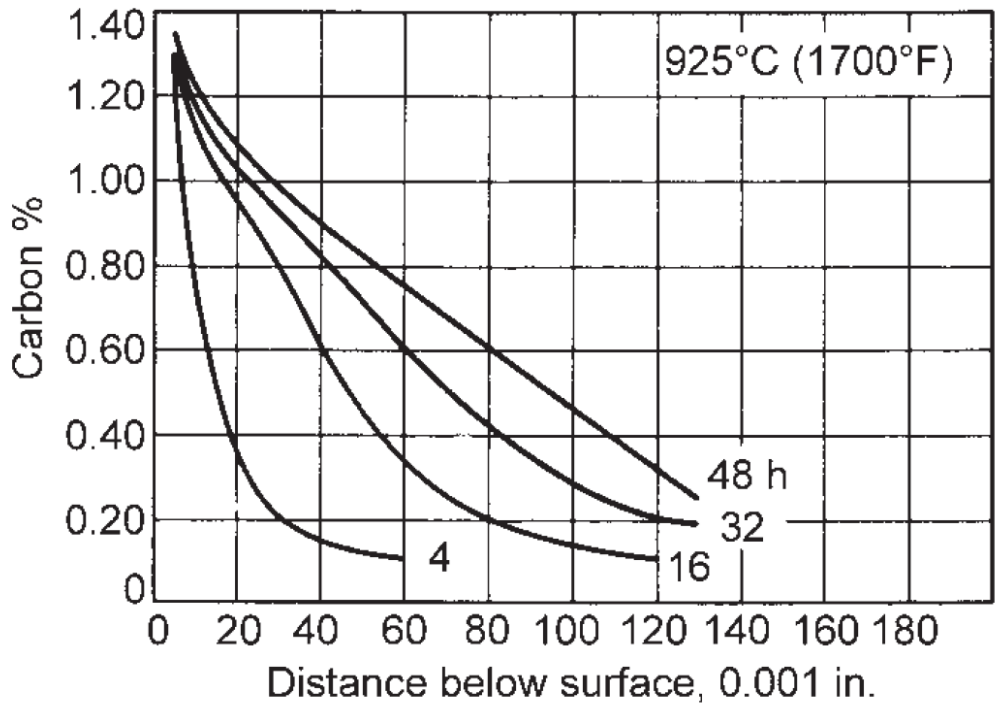

Figure 4: Carbon content vs. depth is steel pack carburized at 925C[42]

2.3.2: Gas Carburization

Gas carburization is a carburizing process in which the carbon rich environment is provided by a gaseous atmosphere containing a variety of carbonaceous gasses including carbon monoxide, carbon dioxide and methane, as well as some amount of hydrogen and water vapor.[44] These gases can deposit active carbon onto the surface through a variety of reaction pathways shown in equations 4 - 6[45]

$$2CO + Fe \rightarrow C_{active} + CO_2 \quad \text{(Eq 4)}$$

$$CH_4 + Fe \rightarrow C_{active} + 2H_2 \quad \text{(Eq 5)}$$

$$CO + H_2 \rightarrow C_{active} + H_2O \quad \text{(Eq 6)}$$

The composition of the gas carburizing atmosphere is highly variable depending on the specific application but usually contains 15-30% CO, at least an equal amount of H_2, and less than .2% CO_2. Higher levels of the carbonaceous gasses can have negative side effects such as soot deposition.[46]

The rate of carburization and carbon penetration depends on the specific composition of the carburizing atmosphere as well as the temperature at which carburization occurs. A representative sample of the depth of carbon penetration can be seen in **Figure 5.**

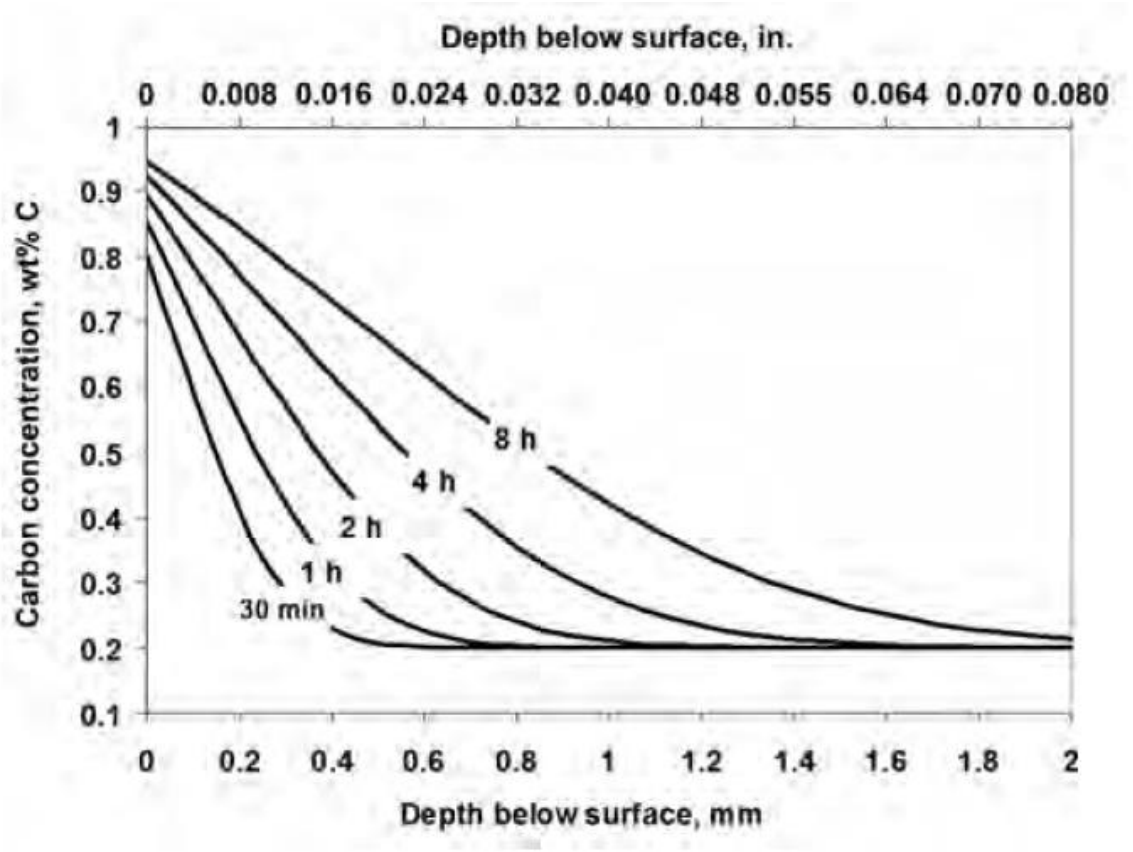

Figure 5: Carbon concentration vs. depth for steel gas carburized at 925C[45]

2.4: Hardness and Heat Treatment

Iron carbon mixtures can take on a wide range of forms including pearlite, bainite, and cementite.[47] Of interest to this work is the formation of martensite. When a mixture of iron and carbon is heated to a temperature above 723C it forms austenite, an FCC form also called gamma iron. If allowed to cool slowly, the austenite decomposes into a range of structures composed primarily of BCC ferrite, also known as alpha iron, and cementite. These structures include pearlite and bainite. The formation of these segregated groupings of ferrite and cementite is a diffusion process that takes time.[48],[49] If the steel is cooled rapidly (on the order of 300C/s) from temperatures above 723C this diffusion process does not have time to occur, the carbon atoms are largely trapped in place, and martensite forms instead.[50] Martensite is a BCT phase of ferrite that is supersaturated with carbon.[51] The primary characteristic of martensite is that it is extremely hard and strong. [52],[53] Martensite is also quite brittle.[54] Martensite also has another very useful property for this thesis. The hardness of martensite increases with increasing carbon content, up to a carbon content of .6wt% C where it essentially becomes constant at around 67 hardness Rockwell C (HRC), and this hardness is dependent only on carbon content and is not affected by the presence of other alloying elements.[51],[4] Measuring carbon content in steels can be quite difficult, however hardness tests are quick and easy to preform and require minimal sample preparation, and are therefore an ideal test for an approximate measure of carbon content in martensitic steels.

Chapter 3: Methods

3.1: Ink preparation and printing

Ink for the production of plain carbon steel and a low nickel steel were produced. Inks were manufactured using powders of 1–5-micron Fe_2O_3 (Sigma Aldrich) , and 5-10 micron NiO (Inframat Advanced Materials) blended with poly (lactic-co-glycolic acid) (PLGA) (Re- somer 824-S) in a 7:3 volume ratio of oxide powder to polymer and mixed with a tri-graded volatility solvent of Dichloromethane (DCM), ethylene glycol- butyl-ether (EGBE), also referred to as 2-Butoxyethanol , and Dibutyl Phthalate (DBP) to manufacture a shear thinning ink. This combination of polymer and solvent base have been studied extensively in prior literature and the benefits are well understood.[32,28,55]

To prepare the ink, first a 'blank' ink was made through combining 1.44g PLGA, 1.99g EGBE, 2.23g DBP, 23.03g DCM, and .24g Soy Lecithin. This 'blank' ink was then left to sit in the fridge for at least 12 hours or until all the components had dissolved leaving a smooth solution. Oxide powders were combined in a separate container. For the plain carbon steel this was 10.48g Fe_2O_3, and for the nickel-steel composition this was 10.25g Fe_2O_3 and .3g of NiO. The blank ink was combined with the oxide mix, stirred by hand, and then mixed in a Flaktek DAC 400.2 VAC-LR speed mixer. Oxide inks were mixed at 500 RPM for 30s, followed by 1000 RPM for 30s, and finally 1500 RPM for 30s. Inks were then allowed to rest for at least 4 hours before being loaded and printed. Prepared inks were loaded into 30ml metal screw driven syringes. Loading was done with the nozzle end of syringe facing upward, and the plunger all the way at the top. The plunger was slowly lowered as ink was poured into the open end of the syringe. Ink would stop being added when the syringe was half full and the syringe would be capped with a Luer tip adapter. Once capped, the plunger was then lowered all the way down, stretching the ink out along the walls of the syringe in an attempt to provide a clear pathway for

trapped air to escape. Once loaded, inks were printed using a Hyrel Engine HR system with an Emo-25 modular head and Luer tip adaptor with an 18-gauge straight Luer tip. 20x20x3mm samples were prepared for the experiment. Samples were printed with a print speed of 15mm/s, a layer height of .3mm, and an extrusion multiplier of 1.6. This means that each printed line contained 1.6 times the amount of ink needed to perfectly fill the void under the Luer tip during each pass, and the slicer settings were adjusted such that there was a 15% overlap between adjacent lines. In print testing, the most important print setting variable in relation to print quality was the ratio between nozzle diameter and layer height. Any ratio less than ~1:1 or greater than ~3:1 yielded unsatisfactory prints. If the ratio was less than 1:1 then inks did not fully fill in the void below the nozzle as it moved across the print, leading to gaps and voids in the print. If the ratio was greater the 3:1 the ink would eject sideways way from the syringe causing inconsistent line with and compromising dimensional accuracy of the part. The ideal ratio was identified to be ~2.5:1, which provided a good balance between the need to fill the print fully and maintain consistent line width, yielding smooth consistent lines that connected with each adjacent line.

3.2: Furnace Processing of Iron and Iron-nickel Samples

Printed samples were post-processed in an MTI GSL1600X furnace, using ultra high purity (99.9999% pure) argon and hydrogen. The exact temperature and time settings for the furnace are show in **Figure 6.** In general, there are 4 stages to each furnace cycle, a low temperature debind in argon gas to burn off the plastic binder, a middle temperature stage in H_2 to reduce the metal oxides to pure metals, a high temperature sintering stage in argon, and an unpowered cooling phase in argon. During heating to the debinding step, the furnace temperature was increased at a rate of 5°C/min, from debinding to sintering, the temperature was increased at a rate of 10°C/min, after the sintering step the furnace was powered off and allowed to cool to

room temperature. All gasses were kept at 3 PSI gauge pressure and .3 LPM flow rate for the entirety of the run.

Further development on the post processing procedure proposed in prior work, as discussed in section **2.2,** was done for this work. Simulation of reduction was done using modeling in COMSOL Multiphysics to explore the reduction reaction of iron oxides in a hydrogen atmosphere. The minimum temperature for the reduction reaction to take place was found to be 600C, with the rate increasing with temperature. For this work the reduction temperature was increased from 600C to 875C over the course of the furnace run to increase the speed of reduction. Additionally, the maximum temperature was increased to 1100C in order to aid sintering and produce more dense samples. Prior work shows that a higher sintering temperature increases final part density.[34],[35],[36].

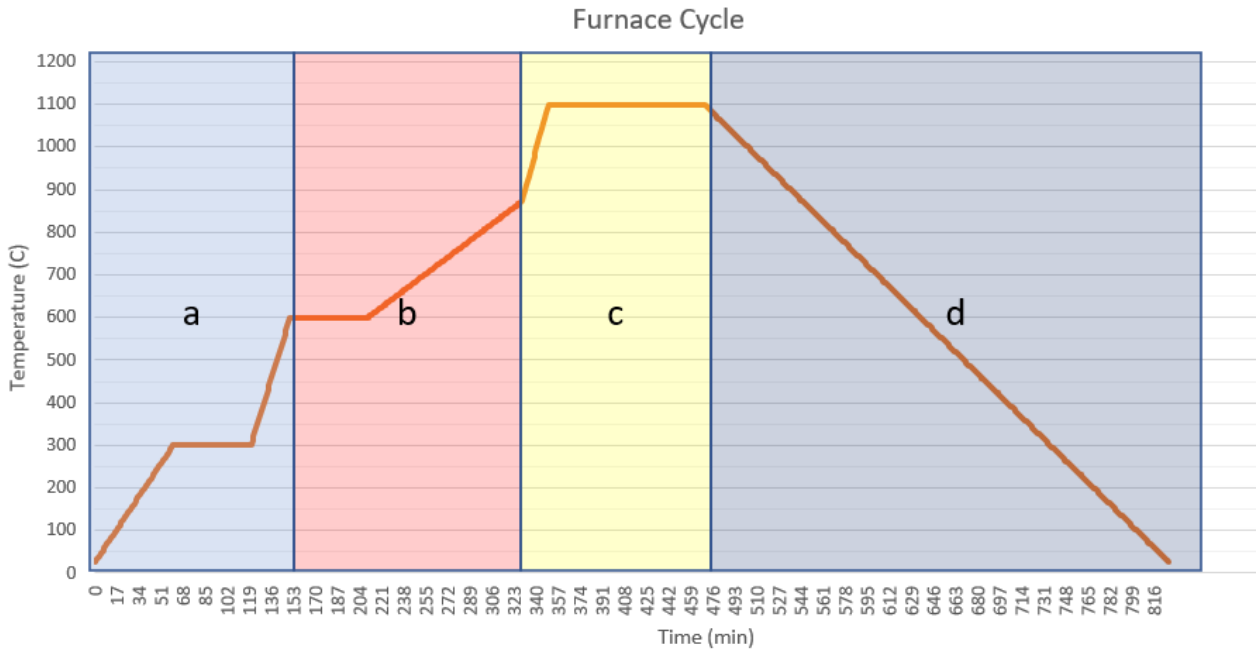

Figure 6: Standard Furnace Processing Route **A:** Debinding. **B:** reducing. **D:** sintering. **E:** cooling

3.3: Furnace Processing for Carburized Steel Samples

Samples intended for carburization were treated very similarly to those that were not carburized, the furnace temperature and time profiles were modified to allow for additional time for the carburization reaction to occur and for carbon to diffuse into the part. This added time is referred to throughout the rest of this work as "carburization time" and represents the time added to the standard processing route specifically to allow time for carburization. This time is represented by segment C in **Figure 7**. The carburizing time was varied between samples and can be seen in **Table 1**. Samples were also subjected to two variations of carburizing, gas and pack carburization.

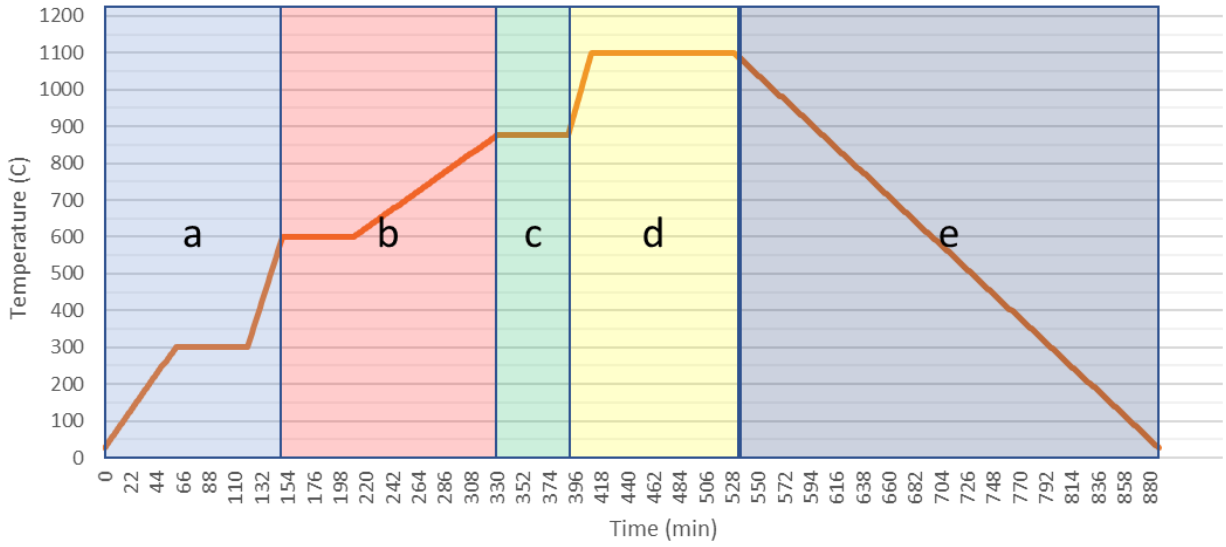

Figure 7: Carburization Furnace Processing Route **A:** Debinding. **B:** reducing. **C:** carburizing, time for this step is variable and can be found in Table 1. **D:** sintering. **E:** cooling

Reduced and carburized samples were subject to heat treatment in a Thermolyne model FD1535M bench top box furnace. Samples were heated to 450°C, then removed from the furnace and coated in PCB anti-scale compound and returned to the furnace. They were then heated to 875°C, held for one hour, and then immediately quenched in water. Both before and after heat treating, samples were tested for hardness using a LECO AMH55 hardness tester. After heat treating, samples were ground to the middle of their thickness using silicon carbide paper before hardness testing in order to evaluate hardness far from the sample surface. This paper uses hardness data as an intermediary to determine carbon content of the steel samples produced. Hardness is an effective measure of carbon content in fully martensitic steel.[4] The hardness of martensite is related only to the carbon content of the steel and not related to the presence of other alloying elements. The downside to using hardness as a measurement of carbon content in steel is that is cannot effectively measure carbon content above .6 wt%. Any martensite with a carbon content above .6 wt% will have a hardness of approximately 67 HRC.[51]

Table 1: Sample Composition, Carburization method and Time

Sample Number	Alloy	Carburization method	Carburization Time (hr)
1	Plain Steel	Pack	0
2	Nickel steel	Pack	0
3	Plain Steel	Pack	.5
4	Nickel steel	Pack	.5
5	Plain Steel	Pack	1
6	Nickel steel	Pack	1
7	Plain Steel	Pack	2
8	Nickel steel	Pack	2

Table 1 Continued

9	Plain Steel	Pack	4
10	Nickel steel	Pack	4
11	Plain Steel	Pack	8
12	Nickel steel	Pack	8
13	Plain Steel	Pack	12
14	Nickel steel	Pack	12
15	Plain Steel	Pack	16
16	Nickel steel	Pack	16
17	Plain Steel	Gas	0
18	Nickel steel	Gas	0
19	Plain Steel	Gas	.5
20	Nickel steel	Gas	.5
21	Plain Steel	Gas	1
22	Nickel steel	Gas	1
23	Plain Steel	Gas	2
24	Nickel steel	Gas	2

3.3.1: Gas Carburization Method

In gas carburized samples, CO gas was introduced to the furnace environment during processing during the reduction and carburization stages (b and c in **Figure 7)**. During reduction and carburization, the furnace atmosphere was 15% CO and 85% H_2 by volume. Both gasses were kept to 3 PSI gauge pressure and the total combined flow rate was kept to .3 LPM. CO gas was introduced during the reduction stage as CO is a reducing gas.[56] and therefor there is an opportunity to both reduce and carburize the samples at the same time yielding a more efficient process.

3.3.2: Pack Carburization Method

Pack carburized samples were placed in the center of a boat surrounded on all sides by pack carburizing compound. The pack carburizing compound consisted of 85% powdered charcoal, 15% Calcium Carbonate by weight. For our purposes calcium carbonate is used as a less toxic alternative to the industry standard barium carbonate.[42] Samples were placed into an alumina boat with an approximately 5mm layer of pack carburizing compound on the bottom of the boat. Samples were placed on top of this layer and then covered with more pack carburizing compound until the boat was full, with approximately an additional 5mm of compound covering the samples. There was approximately 15mm of carburizing compound around the samples on all sides but the top and bottom. Other than the addition of carburizing time to the furnace procedure nothing else about the furnace atmosphere or environment was changed.

Chapter 4: Results

4.1: Reduction, Sintering, and Densification

Sintered samples presented a fully metallic structure, with well dispersed alloying elements as seen in **Figure 8.** After furnace post processing the samples shrunk on average 45.3% in the X and Y direction (perpendicular to the build direction) with a standard deviation of 2.7% and 41.7% in the Z direction (parallel to the build direction) with a standard deviation of 5.5%, as determined by geometric measurement. This yields a total volumetric shrinkage of 82.6%. Samples lost on average 47.6% of their mass.

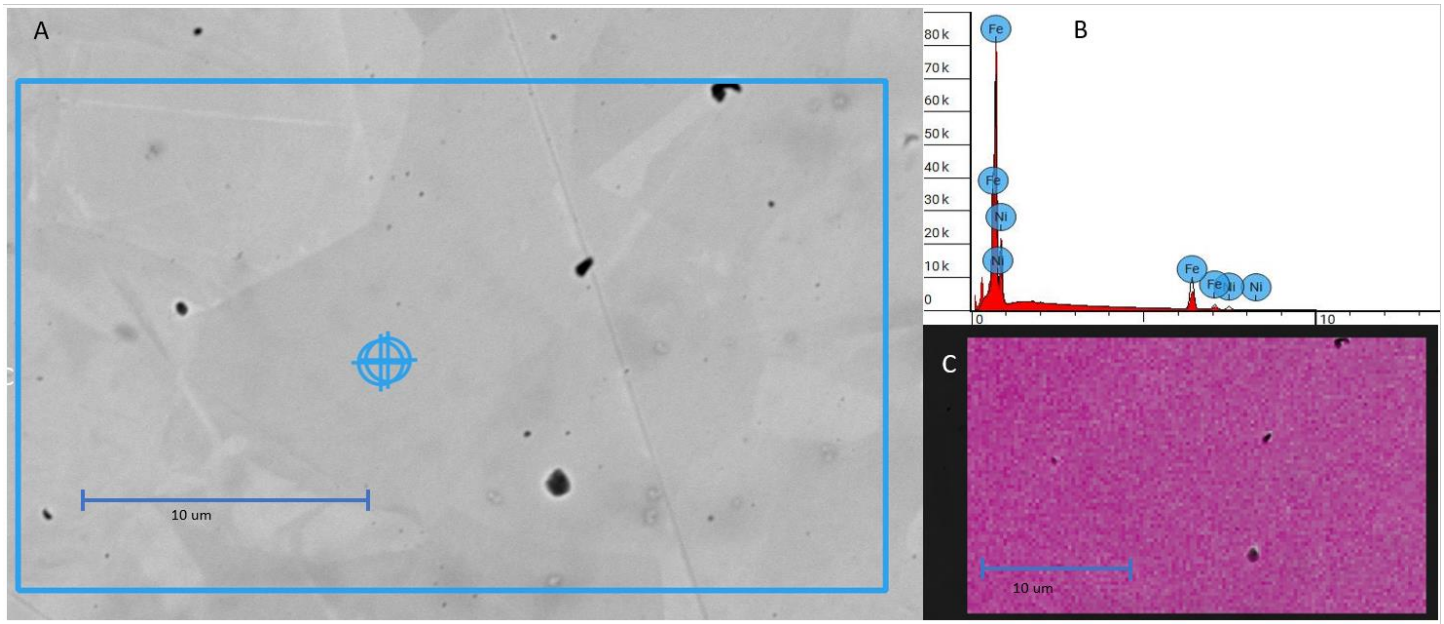

Figure 8: A: SEM image of sample 6. **B**: EDS Spectra. **C**: EDS Fe-Ni Composite Element Map.

The theoretical mass loss and volumetric were calculated to be 39% and 72% respectively, meaning that samples lost more mass and volume than was theoretically predicted. The theoretical values for shrinkage are calculated assuming the printed green body consists only of PLGA, soy

lecithin, and oxides. It is possible that the green body contains retained solvent and the loss of these solvents during furnace post processing is responsible for the excess mass and volume losses.

The average density across all samples was 90.5% of theoretical full density for their respective alloys. Density was measured using Archimedes density testing.[57] There was no significant difference in density between alloys or processing procedure. Plain steel samples had an average density of 89.9% of theoretical full density with a standard deviation of 4.4%, nickel steel samples had an average density of 91.0% of theoretical full density with a standard deviation of 4.9%. Pack carburized samples had an average density of 91.0% with a standard deviation of 4.3% and gas carburized samples had an average density of 89.3% with a standard deviation of 4.6%. Prior work has shown that struts or filaments of metal oxide DIW ink sinter to near full density. However challenges have occurred when attempting to manufacture bulk solid parts.[27,29] The DIW method is often used to create lattice structure, and the highest bulk densities achieved are on the order of 70%.[58]

The information above suggests that new sources of porosity emerge when going from filament like structures to bulk solid parts. One possible new source is errors or inefficiencies in the printing process. This agrees with the observations by the author of the study presented here. Some prior work has been done on this issue, and with careful controls to make inks more printable solid parts in the range of 90% density can be produced when starting with metal powders.[59] This work has not been extended to using oxide precursors. The largest issue experienced in printing samples for this paper was loading the inks into the printing syringe without introducing air bubbles that would then cause voids in the print when there was interrupted ink flow. Despite these factors the work in this paper represents a significant increase in the upper limits for density of solid bulk parts produced through the oxide DIW processes.

This increase in density can likely be attributed to 3 main factors, first an increase in the relative amounts of EGBE and DBP in the solvent mixture. Prior literature has used a EGBE to DBP ratio of 2:1, we have brought this ratio to 1:1.1 by increasing the amount of DBP. We have also raised the relative amounts of EGBE and DPB relative to PLGA as compared to prior literature as well.[27,28,29] Second is the use of 1% Soy Lecithin by volume as a dispersant to increase the flow properties of the ink. Both of these changes are an attempt to balance the stiffness of the printed ink with its ability to flow through the nozzle. Stiffer inks print more reliably and hold their shape after leaving the nozzle. However, if inks are made too stiff, they have a greater tendency to jam in the nozzle, causing the print to fail. By adding a dispersant and changing the solvent mix, we were able to allow stiffer inks to flow through the nozzle without jamming. The last item is the careful selection of the ratio between nozzle diameter and layer height discussed in the methods section. This provides more material than is needed to fill the space beneath the nozzle on each pass, causing it to squeeze outwards, filling any potential gaps or errors from previous passes. The importance of this parameter is supported by prior work in the field.[60]

4.2: Hardness and Carburization

Samples were tested for hardness both before and after heat treating. The pre-heat treat hardness test was done on the sample surface as-is after the furnace processing. After heat treating, samples were ground to the midpoint of their thickness and polished with 4000 grit abrasives, then hardness tested. Very little difference in hardness was seen between the plain carbon and the nickel steel samples. This is in line with what would be expected for a fully martensitic steel as the hardness is dependent only on the carbon content and not on any alloying elements.[51] The average hardness across all samples before heat treating was 21.18 with a standard deviation of 1.86 HRC. The average pre-treatment hardness for plain carbon steel samples was 22.0 HRC with a standard deviation of 1.34 HRC. For nickel steel samples the average was 20.2 HRC with a standard

deviation of 1.9 HRC. Pack carburized samples had an average untreated hardness of 20.9 HRC with a standard deviation of 2.0 HRC. Gas carburized samples had an average hardness of 21.4 HRC with a standard deviation of 1.6 HRC This hardness value is in line with the values expected for annealed carbon steels.[61] After heat treatment, the average hardness of the samples was 62.82 HRC with a standard deviation of 1.98, values for each composition and carburizing time are seen in **Figure 9.**

These results show that all samples were carburized through their thickness to at or beyond .6wt% C. Above .6wt% C steels achieve their maximum hardness of around 63 HRC. Beyond .6wt% C hardness is no longer a reliable measure of carbon content.[51] However .6wt% C is reaches the maximum possible hardness for low alloy or plain carbon steels and therefore is suitable for applications where hardness is the desired property. This hardness value can certainly be reduced by changes in the heat treatment procedure, including by tempering of the steel.[62,63]

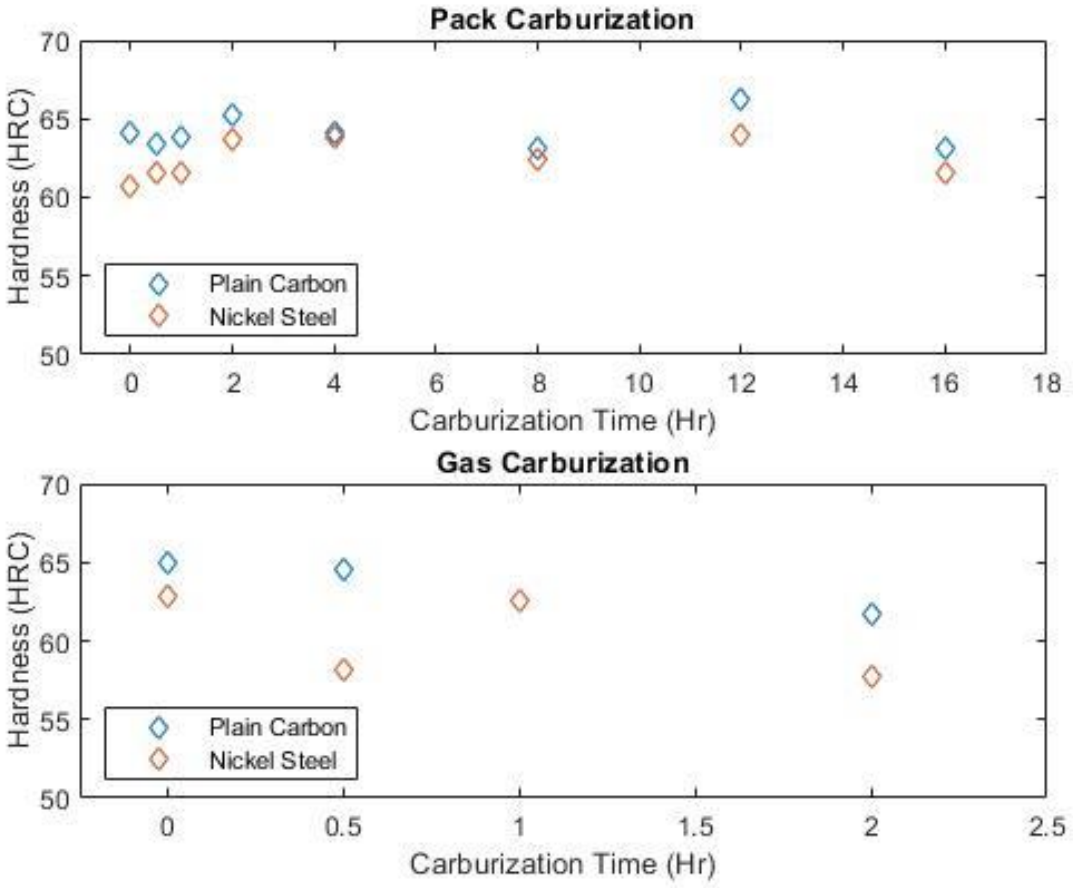

Figure 9: sample hardness vs. carburization method and time

It is important to note that the times listed in **Table 1** are the "carburizing times" where a carburizing time of zero represents a furnace run with time and temperature settings that will yield satisfactory sintering and reduction of oxides based on prior work in the field[27] and experience of the authors. A carburizing time above zero indicates additional time added to the furnace process that is not strictly necessary for reduction or sintering. The results from hardness testing make it apparent that carburization is occurring outside of these times. To better compare samples produced in this study to the solid samples carburize in prior literature, samples from this study were evaluated for their "maximum carburizing time" this time represents the

maximum possible amount of time in which carburization could possibly occur and it is defined as the time during which samples were exposed to the carburizing environment and above 800C, which is the minimum temperature for carburization to occur at any appreciable rate.[64] Because the pack carburized samples were encased in the carburizing compound for the entirety of the run this maximum carburizing time is much higher for them than it is for the gas carburized samples. The hardness results indicate that .6% C is the lower possible bound for carbon content in the samples, and the maximum carburizing time represents the longest possible time over which the samples could have been carburized, therefor combining these two values give the lowest possible rate of carburization that samples underwent. Hardness versus maximum carburizing time is shown in **Figure 10.**

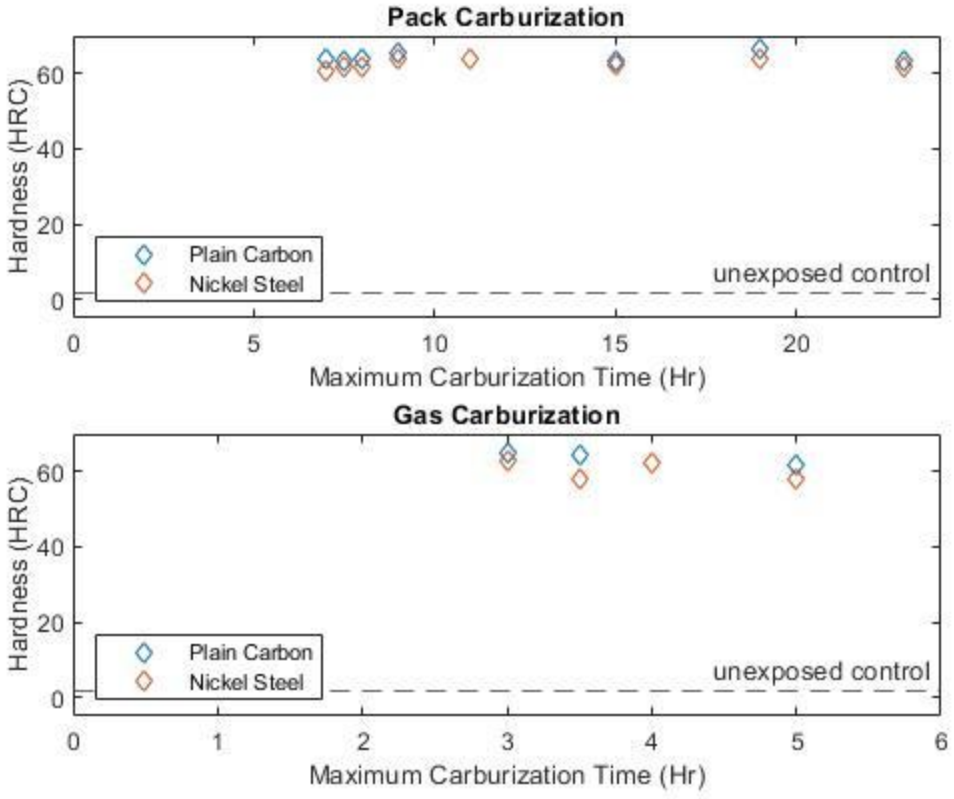

Figure 10: sample hardness vs. carburization method and maximum carburizing time. Dashed line represents hardness of samples never exposed to a carburizing environment

The values presented here indicate significantly faster carburization than has been seen in previous studies. Traditionally carburization is done to solid metal components, and in the case of this study samples had been reduced, but not yet exposed to high enough temperatures for sintering to occur when they were carburized. Samples in this study displayed carburization rates between 1.4 and 5 times faster than the rates presented in prior work.[45],[42],[6],[41]. One possible reason for this increased rate is that the porous structure of the samples during carburization allowed CO gas to penetrate the part, increasing the available surface area for carbon deposition and reducing the need for carbon atoms to diffuse through metal as shown in **Figure 11.**

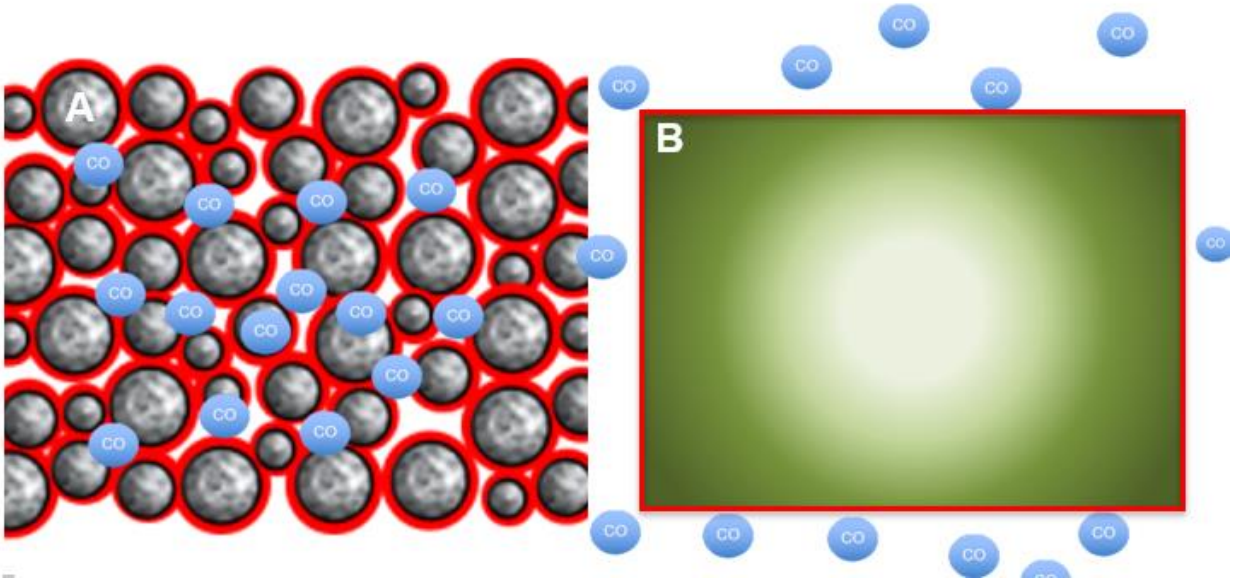

Figure 11: Carburization process, red outlines represent zones of active carbon deposition by CO gas. **A:** Carburization of porous reduced structure. **B:** Carburization of solid metal, gradient represents inward carbon diffusion

4.2.1: Possible Novel Reaction Pathways for Pack Carburization

The conventional pack carburizing process discussed in *Section 2.3.1* is not what is happening to the samples presented in this paper. Primarily because the carbon in the pack carburizing compound in this process is never exposed to atmospheric O_2, the furnace environment is always either pure hydrogen or pure argon. Additionally, because the pack carburizing content is present in the entirety of the furnace run, it is exposed to much higher temperatures than would be typically used for pack carburizing. There are two possible pathways by which active carbon is introduced to the part. The first possibility is that oxygen from the oxides reacts with solid carbon to form CO,[65] much in the same way that coke reacts with iron ores in a blast furnace. This may happen either directly from interactions between the solid carbon and the oxides, or H_2O produced from the oxide reduction in H_2 may react with the carbon to create CO. Both these reactions can happen through numerous pathways as the Fe_2O_3 reduces through multiple oxide forms to eventually become metallic Fe. Potential pathways for these reactions are shown in equations 7 through 10

$$FeO + C \rightarrow Fe + CO \quad \text{(Eq 7)}$$

$$FeO + H_2 \rightarrow Fe + H_2O \quad \text{(Eq 8)}$$

$$H_2O + C = CO + H_2 \quad \text{(Eq 9)}$$

$$2CO + Fe \rightarrow C_{active} + CO_2 \quad \text{(Eq 10)}$$

A second possibility is that when the calcium carbonate decomposes at high temperature, the CO formed from this decomposition then provides the active carbon atoms needed for carburization. The furnace process reaches a temperature of 1100°C, more than high enough to decompose calcium carbonate[66] and produce CO_2 which then can react with the solid surrounding

carbon to form CO. A side effect of this is that the pack carburizing compound used with this method cannot be re-used for additional runs as is typical in industrial processes, all the calcium carbonate in this method fully decomposes. This was confirmed by attempting furnace trials with previously used pack carburizing compound and the resulting samples only achieved a hardness of approximately 20 HRC. This confirms the importance of the calcium carbonate as an important part of the carburizing compound and it's break down during a particular run, however it does not prove that break down is the cause of the carburization. It is known that in traditional pack carburizing processes the energize is not broken down. In commercial pack carburization the temperatures are kept below the decomposition temperature of the energizers. Therefore, in the conventional process no CO is produced through carbonate decomposition, and the process still is able to produce carburized parts. This shows it is possible to carburize parts without the breakdown of the carbonate energizer.

To better determine the particular mechanism, two samples, one plain carbon steel and one nickel steel sample, were reduced in the furnace. This produced a fully metallic sample with no oxides present. These samples were then placed in the furnace again and subjected to an identical carburizing furnace process as samples 1 and 2 in **Table 1**, and then heat treated. The samples had a hardness of 45.1 and 46.2 HRC, respectively. These values are significantly different from those of samples 1 and 2 which were exposed to the same carburizing environment, with an end hardness value of 64.1 and 60.7 respectively. This strongly suggests that the oxides in the green body structures are at least partly responsible for the generation of the CO needed for pack carburization, presenting a potential novel pathway for carburization.

Chapter 5: Conclusion

We have demonstrated that a variety of carbon steel alloys can be produced by DIW printing of oxide precursors, and thermal post processing. This presents a method to additively manufacture carbon steel alloys that have proven consistently difficult to produce through other AM methods. Adding carbon steels to the AM toolset brings with it the ability to tune the mechanical properties of printed structures through variations in the post processing and heat-treating procedure to achieve the desired behavior. This can be achieved without significantly increasing the furnace post processing time needed as compared to non-carburized alloys, as the carburization appears to occur at a significantly faster rate than has been reported in previous literature. The precursor oxides can be obtained cheaply and allow for a highly flexible alloy composition in batches of almost any size. The work also makes significant progress on the production of high-density bulk solid parts produced by DIW printing allowing for significantly more dense solid structures than previously reported.

Appendix A: AM Package for Austere Military Environments

The practical application the author envisions for Oxide DIW printing is to provide a robust metal AM solution suitable for austere environments and military deployment to remote locations. Part of this research was funded by the United States Special Operations Command (US SOCOM) and so the use case of this technology was targeted towards their application needs. The U.S. Military currently employs a range of plastic 3D printers in deployed environment. However, for a number of reasons, no metal AM solutions currently exist suitable for forward deployment. Some of the limiting factors are size, weight, power requirements, sensitive or delicate laser equipment, and metal powders which are difficult to transport and store.

the Oxide DIW system overcomes a number of these limitations, for one, oxide powders are stable under ambient conditions, and the inks can be manufacture behind the lines and shipped out to forward deployed locations. The total system is small, lightweight, and can be built rugged enough to be air droppable. Additionally, the extrusion-based approach is incredibly flexible and can be used for far more than just the oxide inks presented here. The Hyrel printer systems are also modular and can make use of multiple heads to employ various types of printing. Most relevant to this use case is the polymer 3D printer head that enables Special Operators to be able to make both plastic and metal parts on the same printer.

The Kacher lab is presenting a prototype package to US SOCOM with a wide range of capabilities. 3 fundamental capability types are being presented: Oxide DIW, polymer Fused Deposition Modeling, and putty extrusion. Putty extrusion is being used to demonstrate the capability to 3D print C4 plastic explosives, a very common military explosive caried by Special Operations troops. Oxide DIW will be used to demonstrate the printing of high carbon steels to

manufacture hardened M4 disconnectors, part of the trigger mechanism on the U.S. standard issue carbine. FDM printing will be used to show the ability to print carbon fiber filled PETG to manufacture a variety of attachments for the M4 carbine, including a flashlight holder and barrel-mounted shooting stabilizer. The PETG will also be printed into Blank Firing Discriminators (BFDs) for the standard issue U.S. Belt fed machine guns, the M249 and M240B. BFDs adapt a belt fed machine gun to fire blank rounds for training missions. The FDM head of the Hyrel printer will also be used to print Ultrafuse 316L filament from BASF. Ultrafuse consists of particles of stainless steel 316L suspended in a thermoplastic binder that can be printed on an FDM printer. It has many of the drawback of using metal powders, and only is available in one alloy, but the geometric complexity available through FDM printing currently exceeds what the authors can achieve through DIW. Ultrafuse filament will be printed into additional BFDs and M4 Disconnectors. Putty printing will be used to manufacture mock shape charges out of Super Sculpey model clay.

The entire system will consist of an integrated furnace and printer mounted in a welded aluminum frame; Gas tanks will be mounted to the back of the system. The current system uses the exact printer and furnace described in the methods section and is show in **Figure 12.** It is intended be powered by a standard military 5 Kw generator.

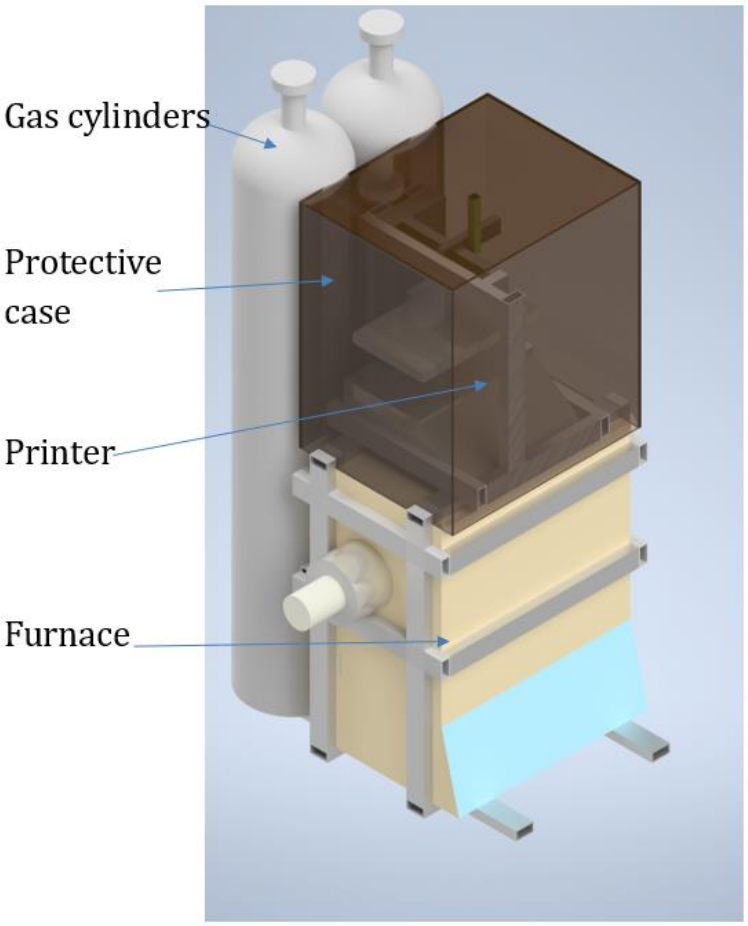

Figure 12: Generation 1 prototype of a multi-material AM system

The system as currently designed has several significant drawbacks. The two most important ones are first the need for tanks which must be replenished, and the extremely limited furnace size, which limits metal part sizes to approximately 3inch diameter by 6 inches long. A generation 2 prototype will have a larger furnace, a hydrogen generator to generate hydrogen from water, and be more robust to allow it to be deployable for parachute deployment. The design for this system is show in **Figure 13.**

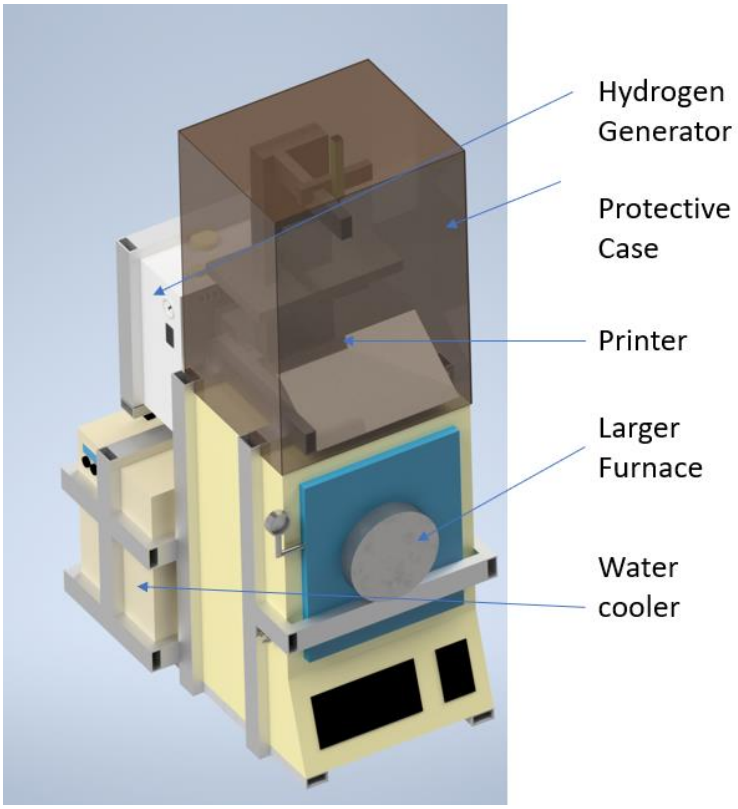

Figure 13: Generation 2 Prototype

Appendix B: Promising Alloys for Future Study

In the process of developing this work, numerous alloys were test printed. These alloys were sintered and appeared metallic but were not extensively characterized, as such these alloys should be considered likely candidates for future analysis to confirm these preliminary results. No data were collected to confirm that these alloys were fully sintered or reduced. Two different alloy steel compositions were made. First with a final weight composition of 3% Ni, 3% Co, and 1.1% Cu. Second with a final weight composition of 3% Ni, 3% Co, 1.1% Cu, .43% Mn, .1% Cr, and .1% Mo. In both cases the remaining mass was entirely Fe. Samples were also manufactured out of stainless 316L. 316L is desirable in some applications for its low carbon content, and it is notable in our application that the carbon content isn't just low but zero. An alloy with potential biomedical applications was also made with a final weight composition of 65% Co, 28% Cr, 6%

Mo, and 1% Ni. This information is included purely for the benefit of those who may want to expand upon the work in this thesis and apply it to new alloys.

Bibliography

1. *Mineral commodity summaries 2021*. *Mineral commodity summaries 2021* 200 http://pubs.er.usgs.gov/publication/mcs2021 (2021) doi:10.3133/mcs2021.
2. Steel - Raw Materials. https://science.jrank.org/pages/6483/Steel-Raw-materials.html.
3. Iron and Steel Production. https://www3.epa.gov/ttnchie1/ap42/ch12/final/c12s05.pdf
4. Calik, A., Duzgun, A., Sahin, O. & Ucar, N. Effect of Carbon Content on the Mechanical Properties of Medium Carbon Steels. *Z. Für Naturforschung A* 65, 468–472 (2010).
5. Madu, K. & Uyaelumuo, A. E. *Parametric Effects of Carburization Time and Temperature on the Mechanical Properties of Carburized Mild Steel*. https://papers.ssrn.com/abstract=3209937 (2018) doi:10.2139/ssrn.3209937.
6. Oluwafemi, O., Oke, S., Otunniyi, I. & Aramide, F. Effect of carburizing temperature and time on mechanical properties of AISI/SAE 1020 steel using carbonized palm kernel shell. *Leonardo Electron. J. Pract. Technol.* 14, 41–56 (2015).
7. Moore, M. A. The relationship between the abrasive wear resistance, hardness and microstructure of ferritic materials. *Wear* 28, 59–68 (1974).
8. Husaini, Ali, N., Hamza, J. K. & Sofyan, S. E. Effects of welding on the change of microstructure and mechanical properties of low carbon steel. *IOP Conf. Ser. Mater. Sci. Eng.* 523, 012065 (2019).
9. Odebiyi, O. S., Adedayo, S. M., Tunji, L. A. & Onuorah, M. O. A review of weldability of carbon steel in arc-based welding processes. *Cogent Eng.* 6, 1609180 (2019).
10. Konda Gokuldoss, P., Kolla, S. & Eckert, J. Additive Manufacturing Processes: Selective Laser Melting, Electron Beam Melting and Binder Jetting—Selection Guidelines. *Materials* 10, 672 (2017).
11. Wohlers, T. T. & Caffrey, T. *Wohlers report 2014: 3D printing and additive manufacturing state of the industry annual worldwide progress report*. (Wohlers Associates, 2014).
12. Knieps, M. S., Reynolds, W. J., Dejaune, J., Clare, A. T. & Evirgen, A. In-situ alloying in powder bed fusion: The role of powder morphology. *Mater. Sci. Eng. A* 807, 140849 (2021).
13. Sun, S., Brandt, M. & Easton, M. 2 - Powder bed fusion processes: An overview. in *Laser Additive Manufacturing* (ed. Brandt, M.) 55–77 (Woodhead Publishing, 2017). doi:10.1016/B978-0-08-100433-3.00002-6.
14. Bracken, J. *et al.* Design for metal powder bed fusion: The geometry for additive part selection (GAPS) worksheet. *Addit. Manuf.* 35, 101163 (2020).
15. Seltzman, A. H. & Wukitch, S. J. Resolution and geometric limitations in laser powder bed fusion additively manufactured GRCop-84 structures for a lower hybrid current drive launcher. *Fusion Eng. Des.* 173, 112847 (2021).
16. Ariyama, T., Sato, M., Nouchi, T. & Takahashi, K. Evolution of Blast Furnace Process toward Reductant Flexibility and Carbon Dioxide Mitigation in Steel Works. *ISIJ Int.* advpub, ISIJINT-2016-210 (2016).

17. Fischer, P. *et al.* Temperature measurements during selective laser sintering of titanium powder. *Int. J. Mach. Tools Manuf.* 44, 1293–1296 (2004).
18. Chen, Z. *et al.* Thermodynamic evaluation for reduction of iron oxide ore particles in a high temperature drop tube furnace. *Ironmak. Steelmak.* 47, 173–177 (2020).
19. Zhang, L. *et al.* Metallic iron formed by melting: A new mechanism for magnetic highs in pseudotachylyte. *Geology* 46, 779–782 (2018).
20. Aumayr, C., Platl, J., Zunko, H. & Turk, C. Additive Manufacturing of a Low-alloyed Engineering Steel. *BHM Berg- Hüttenmänn. Monatshefte* 165, 137–142 (2020).
21. Hearn, W. Laser Based Powder Bed Fusion of Plain Carbon and Low-Alloy Steels: Microstructure and Processability. (Chalmers University of Technology, 2021).
22. Saewe, J., Carstensen, N., Kürnsteiner, P., Jägle, E. A. & Schleifenbaum, J. H. Influence of increased carbon content on the processability of high-speed steel HS6-5-3-8 by laser powder bed fusion. *Addit. Manuf.* 46, 102125 (2021).
23. Bates, P. & Tony, R. Safety Considerations for Additive Manufacturing and 3-D Printing.
24. Ron, T. *et al.* Environmental Behavior of Low Carbon Steel Produced by a Wire Arc Additive Manufacturing Process. *Metals* 9, 888 (2019).
25. Desktop Metal. Studio System Design Guide. *Desktop Metal* https://www.desktopmetal.com/resources/bmd-design-guide.
26. Markforged. Markforged Metal 3D Printer: The Metal X 3D Printing System. *Markforged* https://markforged.com/3d-printers/metal-x.
27. Jakus, A. E., Taylor, S. L., Geisendorfer, N. R., Dunand, D. C. & Shah, R. N. Metallic Architectures from 3D-Printed Powder-Based Liquid Inks. *Adv. Funct. Mater.* 25, 6985–6995 (2015).
28. Ahn, B. Y. *et al.* Printed Origami Structures. *Adv. Mater.* 22, 2251–2254 (2010).
29. Koube, K. D., Sloop, T., Stiers, C. D., Sim, H. & Kacher, J. Fabrication of 3D printed complex concentrated alloys using oxide precursors. *Addit. Manuf. Lett.* 1, 100015 (2021).
30. Ellingham, H. J. T. Reducibility of oxides and sulphides in metallurgical processes. *J. Soc. Chem. Ind.* 125–133 (1944).
31. Birks, N., Meier, G. H. & Pettit, F. S. Introduction To The High-Temperature Oxidation of Metals (2nd Edition) (2006). *Scribd* https://www.scribd.com/document/204739422/Birks-N-Meier-G-H-Pettit-F-S-Introduction-to-the-High-Temperature-Oxidation-of-Metals-2nd-Edition-2006-338s.
32. Kenel, C., Casati, N. P. M. & Dunand, D. C. 3D ink-extrusion additive manufacturing of CoCrFeNi high-entropy alloy micro-lattices. *Nat. Commun.* 10, 904 (2019).
33. Smith, J. T. Diffusion Mechanism for the Nickel-Activated Sintering of Molybdenum. *J. Appl. Phys.* 36, 595–598 (1965).
34. Huber, D., Vogel, L. & Fischer, A. The effects of sintering temperature and hold time on densification, mechanical properties and microstructural characteristics of binder jet 3D printed 17-4 PH stainless steel. *Addit. Manuf.* 46, 102114 (2021).

35. Pandya, S., Ramakrishna, K. S., Raja Annamalai, A. & Upadhyaya, A. Effect of sintering temperature on the mechanical and electrochemical properties of austenitic stainless steel. *Mater. Sci. Eng. A* 556, 271–277 (2012).
36. Sung, H.-J., Ha, T. K., Ahn, S. & Chang, Y. W. Powder injection molding of a 17-4 PH stainless steel and the effect of sintering temperature on its microstructure and mechanical properties. *J. Mater. Process. Technol.* 130–131, 321–327 (2002).
37. Innes, J. HISTORICAL NOTES ON THE MECHANICAL THEORY OF HARDENING. *Sci. Prog. Twent. Century 1919-1933* 21, 681–687 (1927).
38. Kishawy, H. A. & Hosseini, A. Hardened Steels. in *Machining Difficult-to-Cut Materials: Basic Principles and Challenges* (eds. Kishawy, H. A. & Hosseini, A.) 9–54 (Springer International Publishing, 2019). doi:10.1007/978-3-319-95966-5_2.
39. *Transactions: Metallurgy. id., 1916. vii, 498 p., 8 plans*. (1916).
40. Raza, M. A. *et al.* Carburising of Low-Carbon Steel Using Carbon Black Nanoparticles. *Arab. J. Sci. Eng.* 41, 4661–4667 (2016).
41. Elmi Hosseini, S. R. & Li, Z. Pack Carburizing: Properties, Microstructure and Modeling. in (2016).
42. Pack Carburizing. *ASM Handb.* 4A, (2013).
43. The efficacy of carburizing compounds with different carbon source and added industrial energizers for surface treatment of mild steel for mechanical property improvement. *MOJ Appl. Bionics Biomech.* Volume 2, (2018).
44. Chekanskii, V. V. Gas carburizing in an atmosphere of activated endogas without adding excess methane to the furnace. *Met Sci Heat Treat Met Engl Transl U. S.* 27:12, (1986).
45. Rowan, O. K. & Keil, G. D. Gas Carburizing. (2013) doi:10.31399/asm.hb.v04a.a0005799.
46. Sproge, L. & Ågren, J. Experimental and theoretical studies of gas consumption in the gas carburizing process. *J. Heat Treat.* 6, 9–19 (1988).
47. Austenite Martensite Bainite Pearlite and Ferrite structures. https://www.twi-global.com/technical-knowledge/faqs/faq-what-are-the-microstructural-constituents-austenite-martensite-bainite-pearlite-and-ferrite.aspx.
48. Li, S. *et al.* Pearlite formation via martensite. *Compos. Part B Eng.* 109859 (2022) doi:10.1016/j.compositesb.2022.109859.
49. Honda, K. Mechanism of the Formation of Pearlite in Steels. *Nature* 164, 229–230 (1949).
50. van Bohemen, S. M. C. & Sietsma, J. Kinetics of martensite formation in plain carbon steels: critical assessment of possible influence of austenite grain boundaries and autocatalysis. *Mater. Sci. Technol.* 30, 1024–1033 (2014).
51. Brooks, C. R. *Heat Treatment of Ferrous Alloys*. (Hemisphere Publishing Corporation, 1979).

52. Shiota, Y., Tomota, Y., Moriai, A. & Kamiyama, T. Structure and mechanical behavior of heavily drawn pearlite and martensite in a high carbon steel. *Met. Mater. Int.* 11, 371–376 (2005).
53. Winchell, P. G. & Cohen, M. *The Strength of Martensite*. https://apps.dtic.mil/sti/citations/AD0281894 (1962).
54. Krauss, G. Martensite in steel: strength and structure. *Mater. Sci. Eng. A* 273–275, 40–57 (1999).
55. Jakus, A. E., Koube, K. D., Geisendorfer, N. R. & Shah, R. N. Robust and Elastic Lunar and Martian Structures from 3D-Printed Regolith Inks. *Sci. Rep.* 7, 44931 (2017).
56. Dey, S. & Mehta, N. S. Oxidation of carbon monoxide over various nickel oxide catalysts in different conditions: A review. *Chem. Eng. J. Adv.* 1, 100008 (2020).
57. Archimedes' Principle. http://www.physics.smu.edu/~scalise/mechmanual/archimedes/lab.html.
58. Peng, S. *et al.* Additive manufacturing of three-dimensional (3D)-architected CoCrFeNiMn high- entropy alloy with great energy absorption. *Scr. Mater.* 190, 46–51 (2021).
59. Pack, R. C. & Compton, B. G. Material Extrusion Additive Manufacturing of Metal Powder-Based Inks Enabled by Carrageenan Rheology Modifier. *Adv. Eng. Mater.* 23, 2000880 (2021).
60. Jang, S. *et al*. Effect of material extrusion process parameters on filament geometry and inter-filament voids in as-fabricated high solids loaded polymer composites. *Addit. Manuf.* 47, 102313 (2021).
61. Harvey, P. D. & American Society for Metals. *Engineering properties of steel*. (American Society for Metals, 1982).
62. Gebril, M. A., Aldlemey, M. S. & Kablan, A. F. Effect of Tempering on Mechanical Properties and Corrosion Rate of Medium and High Carbon Steel. *Adv. Mater. Res.* 685, 81–85 (2013).
63. Ismail, N. M., Khatif, N. A. A., Kecik, M. A. K. A. & Shaharudin, M. A. H. The effect of heat treatment on the hardness and impact properties of medium carbon steel. *IOP Conf. Ser. Mater. Sci. Eng.* 114, 012108 (2016).
64. Obayashi, K. Carburizing of Steels. in *Encyclopedia of Materials: Metals and Alloys* (ed. Caballero, F. G.) 162–172 (Elsevier, 2022). doi:10.1016/B978-0-12-803581-8.12127-7.
65. Yamazaki, Y. *Gasification Reactions of Metallurgical Coke and Its Application – Improvement of Carbon Use Efficiency in Blast Furnace*. *Gasification for Practical Applications* (IntechOpen, 2012). doi:10.5772/51680.
66. Ingraham, T. R. & Marier, P. Kinetic studies on the thermal decomposition of calcium carbonate. *Can. J. Chem. Eng.* 41, 170–173 (1963).